Electrochimica Acta 55 (2010) 6836–6848

Contents lists available at ScienceDirect

Electrochimica Acta

journal homepage: www.elsevier.com/locate/electacta

Comparison of different approaches to the description of the detection limit of ion-selective electrodes

Jerzy J. Jasielec[a], Tomasz Sokalski[a], Robert Filipek[b], Andrzej Lewenstam[a,b,*]

[a] Process Chemistry Centre, c/o Centre for Process Analytical Chemistry and Sensor Technology (ProSens), Åbo Akademi University, Biskopsgatan 8, 20500 Åbo-Turku, Finland
[b] AGH - University of Science and Technology, Faculty of Material Science and Ceramics, Al. Mickiewicza 30, 30059 Cracow, Poland

ARTICLE INFO

Article history:
Received 29 April 2010
Received in revised form 29 May 2010
Accepted 29 May 2010
Available online 4 June 2010

Keywords:
Electro-diffusion
Nernst–Planck–Poisson
Ion-selective electrodes
Potentiometry
Membrane potential
Subnanomolar detection limit
Time-dependency

ABSTRACT

The Nernst–Planck–Poisson (NPP) model is a general approach to the description of the electro-diffusion processes which lead to the formation of the membrane potential. It takes into consideration several parameters of ion-selective electrodes (ISEs) which are ignored in simpler models. This paper presents a critical comparison between the NPP model and simpler models. The influence of different parameters on the detection limit of ISEs is discussed. This is achieved by comparing direct predictions of the models and, in contrast to any earlier treatment, by inverse modelling. This makes it possible to simultaneously find out which set of physical parameters of the system will produce the desired detection limit.

1. Introduction

The formation of the membrane potential of ion-selective electrodes (ISEs) depends on the thermodynamic and kinetic properties of the membrane|solution system, and it is strongly time dependent. Selectivity (K_{IJ}) and detection limit (DL) are constitutive parameters of all ion-selective electrodes.

There is an ongoing and vigorous debate in the ISE literature concerning models describing ISE behaviour in general, and K_{IJ} and DL in particular. There are two main schools of thought. The first one opts for simplicity while the other one stresses generality [1]. The argument that simpler is better applies only if the simpler and the more complicated models are equally general (Ockham's razor).

Advocates of the simple model stipulate that it should be restricted in the following ways: (1) the diffusion coefficients in the membrane should be assumed to be equal for all participating ions, (2) the migration of ions should be disregarded, (3) only two (or, at the most, three) ions should be considered, (4) frequently only ions of the same charge should be taken into account and (5) the model should be restricted to steady-state conditions.

Sometimes proponents of the simple model assume the presence of only two ions of the same charge and time dependence, and sometimes of ions of different charges and steady-state (no time dependence), and from these two cases draw the conclusion that the model (simultaneously) encompasses both different charges and time dependence. This, however, is not true since the assumptions, which have to be made when we consider ions of different charges, are made at the cost of time dependence and vice versa.

The more general (NPP) model takes into account both diffusion (each ion having its own diffusion coefficient both in water and in the membrane), migration, an unlimited number of ions of any charge and time dependence (Table 1).

The ISE models can be roughly divided into three categories: phase boundary models, diffusion layer models, and models including migration. They might also be divided into time-dependent and time-independent (equilibrium and steady-state) models [1].

The debate about the merits of different models has been mostly verbal, and a critical comparison between existing models is lacking so far. In this paper, we compare three models which represent the three main categories: the time-dependent NPP model (NPP), the time-dependent diffusion model (TDM) and the steady-state diffusion model (SDM). We use a dedicated virtual experiment and experimental data to validate competing models.

We hope that the comparison of different models, used for the description of the same well known examples, can exemplify and clarify the basic merits and weaknesses of the different approaches.

* Corresponding author at: Process Chemistry Centre, c/o Centre for Process Analytical Chemistry and Sensor Technology (ProSens), Åbo Akademi University, Biskopsgatan 8, 20500 Åbo-Turku, Finland.
E-mail addresses: alewenst@abo.fi, andrzej.lewenstam@gmail.com (A. Lewenstam).

0013-4686/$ – see front matter © 2010 Elsevier Ltd. All rights reserved.
doi:10.1016/j.electacta.2010.05.083

Table 1
Comparison of the dynamic models presented in this paper.

NPP model	Diffusion models	
	Time-dependent models	Steady-state models
Diffusion, migration (convection)	Diffusion	Diffusion
Exchange and coextraction described by heterogeneous rate constants	Exchange and coextraction described by equilibrium constants	Exchange and coextraction described by equilibrium constants
Potential calculated from electrical field profile	Potential calculated from the phase boundary equation	Potential calculated from the phase boundary equation
Fluxes in all layers are co-dependent (concentrations-potential feedback)	Fluxes in both layers are independent	Fluxes are co-dependent (linear concentration profiles and mass balance)
Ions of any charge	Monovalent ions only	Monovalent ions only
Site distribution depends on electrical field distribution	Sites distribution constant	Sites distribution constant

Note: There is a plethora of models describing ISE behaviour. In this contribution we limit the comparison strictly to models which are directly relevant to the description of low detection limit phenomena. Therefore, some approaches (interesting from the numerical point of view) are not discussed here, e.g. [2].

2. ISE response models

2.1. General model

2.1.1. The Nernst–Planck–Poisson (NPP) model

2.1.1.1. History. The first numerical simulation procedure for the time-dependent NPP problem using an explicit method was developed in 1965 [3]. Later, in 1975, a mixed implicit method (for electric field) and an explicit method (for concentration) similar to [3] was presented [4]. However, due to the explicit nature of the concentration calculation, this method suffered from a very small time step of integration and therefore was very time-consuming.

2.1.1.2. Application of NPP to ISEs. The NPP model offers the most complete and universal description of membranes and related systems (for advanced analysis of the power and limitations of the NPP see [1]).

The application of the NPP model to membrane electrochemistry was presented in a seminal paper [5]. The authors developed an efficient finite difference scheme, totally implicit in time. The resulting set of non-linear algebraic equations was solved using the Newton–Raphson method.

An approach, based upon this idea and dedicated to the general description of ISE behaviour, was later developed [6–9].

The first extension of the NPP model for a two layer system was presented in [10]. The first NPP model implementation where the method of lines (MOL) [11] was used was presented in [12,13]. Later on, MOL extensions of the NPP model for an arbitrary number of layers were developed and implemented in C++ [14] or in MathCad [9] and Matlab [15] scripts.

2.1.1.3. NPP implementation used in this work. The NPP model describes a system consisting of n-layers (phases), inside of which concentration changes of r components (ions or uncharged chemical species) and a change of the electrical field in space and time take place (Scheme 1). The influence of diffusion and migration is expressed by the Nernst–Planck equation for the flux of the ith component inside the jth layer:

$$J_i^j(x,t) = -D_i^j \frac{\partial c_i^j}{\partial x}(x,t) - \frac{F}{RT} D_i^j z_i (c_i^j E^j)(x,t) \tag{1}$$

The continuity equation describes the change of the ion concentrations in time, and the Poisson equation describes the electrical changes caused by the interaction of the species. For convenience, the Poisson equation is replaced by the displacement current equation, as described in [3]. These equations form the following system of evolutionary non-linear partial differential equations (PDE) for r components in n phases:

$$\begin{cases} \dfrac{\partial c_i^j}{\partial t}(x,t) = -\dfrac{\partial J_i^j}{\partial x}(x,t) \quad \text{for } i = 1,\ldots,r; \\ \dfrac{\partial E^j}{\partial t}(x,t) = \dfrac{1}{\varepsilon_j} I(t) - \dfrac{F}{\varepsilon_j} \displaystyle\sum_{i=1}^{r} z_i J_i^j(x,t); \\ x \in [\lambda_{j-1}, \lambda_j] \quad \text{for each phase } j = 1,\ldots,n; \\ t \in [0, t_{\mathrm{END}}] \end{cases} \tag{2}$$

where λ_j is the interface between phases. The above system of PDE is accompanied by boundary and initial conditions.

The mass balance condition at the boundary is expressed by the equality of the fluxes in the boundary point in both phases, $J_i^{\alpha j}(\lambda_j, t) = J_i^{\alpha j+1}(\lambda_j, t)$. The heterogeneous first order rate constants are used to describe the interfacial kinetics at the interface λ_j between phases α_j and α_{j+1}: thus the boundary conditions take a form similar to these described in [16]:

$$J_i^{\alpha j}(\lambda_j, t) = J_i^{\alpha j+1}(\lambda_j, t) = \vec{k}_{i\lambda_j} c_i^{\alpha j}(\lambda_j, t) - \overleftarrow{k}_{i\lambda_j} c_i^{\alpha j+1}(\lambda_j, t) \tag{3}$$

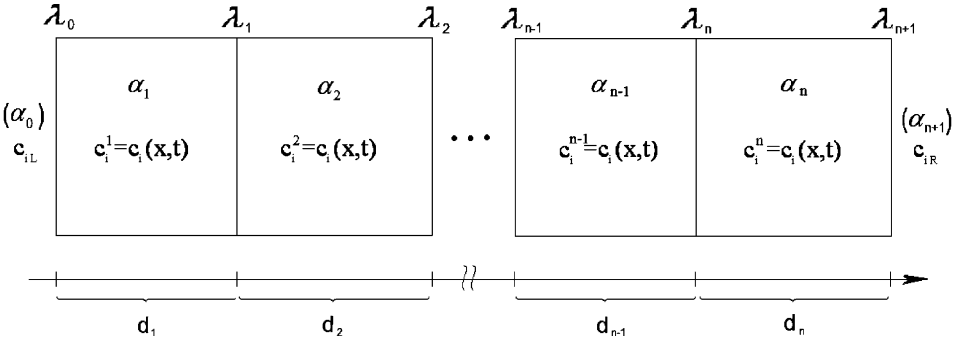

Scheme 1. Scheme of the n-layer system between two solutions.

In simulations of the first point of a calibration curve, an arbitrary initial concentration profile (where the electroneutrality condition is fulfilled) is assumed. For the following calibration points, the initial concentration and the field profiles are based on the final values of the previous steps. This way of setting the initial values reflects the experimental procedure of ISE calibration, i.e. "the history of the ISE".

The method used here is described in detail in Appendix A and in Ref. [14].

2.2. Simplified models

The roots of the diffusion models presented in this paper can be traced back to the original formulation of the so-called diffusion layer model (DLM) [17,18].

All of them share two main assumptions: (a) the potential is governed by the local equilibria described by the Nernst (Nikolskii–Eisenman) equation, and (b) only the Fickian diffusion is considered, i.e. the only source of ion fluxes is the concentration gradient (migration is ignored). This is a rough approximation, since ions are charged and therefore both create and interact with an electrical field.

Diffusion models assume pure diffusion inside both the diffusion layer and the membrane. The concentration change of the ith ion inside the jth layer is given by the continuity equation and Fick's law:

$$\begin{cases} \dfrac{\partial c_i^j}{\partial t}(x,t) = -\dfrac{\partial J_i^j}{\partial x}(x,t) = -D_i^j \dfrac{\partial^2 c_i^j}{\partial x^2}(x,t) \\ x \in]\lambda_{j-1}, \lambda_j[\text{for each phase } j = 1,\ldots,n; \\ t \in [0, t_{\mathrm{END}}] \end{cases} \tag{4}$$

The solution of the diffusion problem given by Eq. (4), along with suitable initial and boundary conditions, belongs to the canon of diffusion and materials engineering and can be found elsewhere, e.g. in the seminal book by Crank [19] and in other books [20,21].

The original DLM was later developed in a number of papers [22–24].

2.2.1. Time-dependent diffusion model (TDM)

The TDM model takes into account only two monovalent ions, the preferred and the discriminated ion, and assumes that their diffusion coefficients in each phase are equal [25]. The authors solved the diffusion problem inside each of the two phases by using the finite difference method. They used the explicit Euler time scheme for two separate uniform grids (in the diffusion layer and membrane) for the space domain, and Euler's method to solve the set of obtained ODEs.

At the left boundary of the first layer, the Dirichlet boundary conditions ($c_i^1(\lambda_0, t) = c_{iL} = \text{const}$) are assumed.

At each time step, the concentration of the ith ion in the kth discretization point of the jth layer ($t + \Delta t$) is expressed as:

$$c_i^{j,k}(t+\Delta t) = c_i^{j,k}(t) + \frac{D_i^j}{\delta_j^2}(c_i^{j,k-1}(t) - 2c_i^{j,k}(t) + c_i^{j,k+1}(t))\Delta t \tag{5}$$

where $\delta^j = (d_j/(N_j - 1))$ represents the distance between two neighbouring grid points.

At the membrane boundaries, the ion concentrations are given by the following equations for equilibrium:

$$c_1(t+\Delta t) = \frac{R_{\mathrm{T}} c_1'(t+\Delta t)}{c_1'(t+\Delta t) + K_{\mathrm{exch}} c_2'(t+\Delta t)},$$
$$]c_2(t+\Delta t) = R_{\mathrm{T}} - c_1(t+\Delta t) \tag{6}$$

where c_i and c_i' are the concentrations inside and outside the membrane phase, R_{T} is the total concentration of anionic sites in the membrane and K_{exch} is the exchange constant.

The potential of the ISE is calculated according to the well known Nikolskii–Eisenman equation:

$$\varphi = \frac{RT}{F} \ln \frac{c_1^{1,\mathrm{N}} + K_{\mathrm{exch}} c_2^{1,\mathrm{N}}}{c_{1\mathrm{R}} + K_{\mathrm{exch}} c_{2\mathrm{R}}} \tag{7}$$

2.2.1.1. Diffusion exchange model (TDM-E). The TDM-E model is analogous to the model described in the previous section but does not assume that the diffusion coefficients of each component in each phase are equal.

In the diffusion layer and inside the membrane the concentration changes are described by Eq. (5).

On the right side of the diffusion layer, the time-dependent concentration is calculated using the equation:

$$c_i^{1,\mathrm{N}}(t+\Delta t) = c_i^{1,\mathrm{N}}(t) + \frac{2D_i^1}{\delta_1(\delta_1+\delta_2)}(c_i^{1,\mathrm{N}-1}(t) - c_i^{1,\mathrm{N}}(t))\Delta t + \frac{2D_i^2}{\delta_2(\delta_1+\delta_2)}(c_i^{2,1}(t) - c_i^{2,0}(t))\Delta t \tag{8}$$

At the boundary points of the membrane, the concentrations of the preferred and discriminated ions are given by the equations for equilibrium distribution:

$$c_1^{2,0}(t+\Delta t) = \frac{R_{\mathrm{T}} c_1^{1,\mathrm{N}}(t+\Delta t)}{c_1^{1,\mathrm{N}}(t+\Delta t) + K_{\mathrm{exch}} c_2^{1,\mathrm{N}}(t+\Delta t)}, \quad c_2^{2,0}(t+\Delta t) = R_{\mathrm{T}} - c_1^{2,0}(t+\Delta t)$$
$$c_1^{2,\mathrm{N}}(t+\Delta t) = \frac{R_{\mathrm{T}} c_{1,\mathrm{R}}}{c_{1,\mathrm{R}} + K_{\mathrm{exch}} c_{2,\mathrm{R}}}, \quad c_2^{2,\mathrm{N}}(t+\Delta t) = R_{\mathrm{T}} - c_1^{2,\mathrm{N}}(t+\Delta t) \tag{9}$$

where R_{T} is the total concentration of anionic sites in the membrane and K_{exch} is the exchange constant.

The potential of the ISE is calculated according to the Nikolskii–Eisenman equation:

$$\varphi(t) = \frac{RT}{F} \ln \frac{c_1^{1,\mathrm{N}}(t) + K_{\mathrm{exch}} c_2^{1,\mathrm{N}}(t)}{c_{1\mathrm{R}} + K_{\mathrm{exch}} c_{2\mathrm{R}}} \tag{10}$$

In order to check whether our implementation of the TDM model is correct, all examples in Ref. [25] were recalculated, giving results which are identical with those in the original publication.

Important note. The authors in [25] assume that the boundary conditions at the interface are given by the continuity equation:

$$\frac{\partial c_i}{\partial t}(x,t) = -\frac{\partial J_i}{\partial x}(x,t) \tag{11}$$

It is true that fluxes at the boundary are continuous (equality of the fluxes), although they are not necessarily differentiable functions. Consequently, Eq. (11) (used for the boundary point), as well as its approximation by finite differences (Eq. (8)), may be mathematically incorrect.

2.2.1.2. Diffusion exchange coextraction model (TDM-EC). For the purpose of this work, the extension of the TDM model was developed with different boundary conditions which consider both exchange and coextraction processes. In the TDM-EC model the diffusion of three monovalent ions (preferred ion, discriminated ion, counter-ion) is considered.

Eqs. (5) and (8) are used as for the TDM-E model (as in the case of the TDM-E model).

At the boundary points of the membrane, the concentrations of the preferred and discriminated ions are given by the following

equations (instead of by Eq. (9)):

$$c_1^{2,0}(t) = \frac{R_T + \sqrt{\Delta_1}}{2 + 2K_{exch}(c_2^{1,N}(t)/c_1^{1,N}(t))}, \quad c_2^{2,0}(t) = c_1^{2,0}(t)K_{exch}\frac{c_2^{1,N}(t)}{c_1^{1,N}(t)}$$
$$c_1^{2,N}(t) = \frac{R_T + \sqrt{\Delta_2}}{2 + 2K_{exch}(c_{2,R}/c_{1,R})}, \quad c_2^{2,N}(t) = c_1^{2,N}(t)K_{exch}\frac{c_{2,R}}{c_{1,R}} \tag{12}$$

where

$$\Delta_1 = R_T^2 + 4\left(1 + K_{exch}\frac{c_2^{1,N}(t)}{c_1^{1,N}(t)}\right)(c_1^{1,N}(t) + c_2^{1,N}(t))c_1^{1,N}(t)K_{coex}$$
$$\Delta_2 = R_T^2 + 4\left(1 + K_{exch}\frac{c_{2,R}}{c_{1,R}}\right)(c_{1,R} + c_{2,R})c_{1,R}K_{coex} \tag{13}$$

For details see Appendix B.

2.2.2. Time-independent model (SDM)

2.2.2.1. SDM1. This model was developed only for monovalent, preferred and discriminated ions and 1:1 complexes, in order to obtain an analytical solution to the equation for the membrane potential [26,27]. The equations and assumptions used in this model are: exchange and coextraction processes, mass balance, charge balance and uniform sites distribution.

The properties of the SDM are identical to those of the TDM except that (a) the SDM is time independent and (b) the fluxes in the diffusion layer and in the membrane are interdependent, which can be described by the mass balance condition.

2.2.2.2. SDM2. Another steady-state model was presented around the same time as the SDM1 [28]. This model is claimed to be very general since it considers any number of ions of any charge. However, a closer inspection shows that only special cases are discussed in this contribution. The possibility of time dependence is also hinted at, but only as an artificial addition.

Later on, a comparison between theory and results obtained using the TDM were presented [24]. It is unclear what the authors meant by the word "theory". This contribution is not discussed here, since the theoretical equation (Eq. (19) in Ref. [24]), which is a special case of the general equation in Ref. [28], does not contain the concentration of the main ion in the inner solution.

3. Calculations

The SDM1 model was implemented in MathCAD 2001i Professional, and SDM2, TDM and NPP in C++. The calculations for the NPP model were done on four HP ProLiant DL 140 G3 servers with two Intel Xeon 2.33 GHz (4 core) processors, 16 GB RAM each under Linux Fedora 8 × 64. For all other models, calculations were made on an IBM PC with an Intel Core2 Duo (2.2 GHz) processor and 2 GB RAM under Windows XP SP3.

The basic virtual experiment was computed for two layers. The first layer, with a thickness $d_1 = 100\ \mu m$, represents the water diffusion layer, and the second ($d_2 = 200\ \mu m$) represents the membrane. The dielectric permeabilities were assumed to be $\varepsilon_1 = 7.07 \times 10^{-10}$ and $\varepsilon_2 = 2.12 \times 10^{-10}$ in SI units, respectively. The temperature was set to $T = 298$ K and the measurement time for each point of the calibration curve was set to 1800 s.

NPP simulations were performed for a system containing four different ions, using the parameters shown in Table 2. High values of heterogeneous rate constants correspond to the Dirichlet boundary conditions. The number of discretization points was set to $N_1 = 60$ and $N_2 = 200$, and the first step of space discretization was set to 10^{-10}.

This system corresponds to the following parameters for the SDM: $R_T = 10^{-4}$ M, $L_T = 2 \times R_T$, $K_{exch} = 10^{-7}$, $K_{coex} = 0.1$, $D_{I,aq} = D_{J,aq} = 10^{-9}$ and $D_{I,m} = D_{J,m} = 10^{-11}\ m^2/s$, $\delta_{aq} = 100\ \mu m$, $\delta_m = 200\ \mu m$, $a_j'' = 0.1$ M, $a_j(\text{bulk}) = 10^{-7}$ M.

In the TDM model, the system is represented by: $d_1 = 100\ \mu m$, $d_2 = 200\ \mu m$, $t = 1800$ s, $K_{exch} = 10^{-7}$, $R_T = 10^{-4}$ M. The diffusion coefficients and ion concentrations are given in Table 2. The number of discretization points was set to $N_1 = 6$ and $N_2 = 21$, and the time step was set to 0.001 s.

Selected parameters were individually varied relative to these settings. All curves were normalized to the point $\{c_{1L} = 10^{-2}$ M, potential = 200 mV$\}$. In Fig. 3, a different set of parameters was used and will be described later on.

4. Results and discussion

It is well known from the abundant literature data [1,26,29–31] that a gradual decrease in the concentration of the main ion in the inner solution of a plastic membrane ISE leads to the improvement (decrease) of the detection limit. However, when the concentration of the main ion in the inner solution becomes too low, a super-Nernstian behaviour, due to the over-compensation of the transmembrane fluxes of ions, is observed.

We performed virtual experiments in order to compare the existing models. The important feature is that we used the same parameters for all the models. A detailed description of these parameters is given in the calculation section above and in Table 2.

4.1. Transient response comparison

In this paragraph, the NPP and the TDM-EC models are compared.

If the measuring time is too short ($t < 300$ s) to allow steady-state to be achieved, it will affect the potential, i.e. the shape of the calibration curve. An ISE with a primary ion concentration in the internal solution equal to 10^{-6} M (ISE6) was used to illustrate this phenomenon (Fig. 1a).

The calibration curves calculated according to NPP and TDM-EC show roughly the same tendencies. At first, with increasing measuring times (t), the detection limit decreases. A further increase of t causes the appearance of a super-Nernstian section, or jump, in the calibration curve. The longer the measuring time becomes, the more this jump moves towards higher concentrations, thus increasing the detection limit.

A closer look at the calibration curves, however, reveals a difference between the models. The TDM-EC curves are much more

Table 2
Ion properties used for calculations (concentrations in mol/dm^3 and all other values in SI units).

i	z_i	D_i^1 [$\times 10^{-9}$]	D_i^2 [$\times 10^{-11}$]	c_{iL}	c_{iM}^1	c_{iM}^2	c_{iR}	$\vec{k}_{i\lambda_0}$	$\vec{k}_{i\lambda_1}$	$\vec{k}_{i\lambda_2}$	$\overleftarrow{k}_{i\lambda_0}$	$\overleftarrow{k}_{i\lambda_1}$	$\overleftarrow{k}_{i\lambda_2}$
I^+	+1	1.0	1.0	[a]	10^{-2}	10^{-4}	[b]	100	100	100	100	100	100
J^+	+1	1.0	1.0	10^{-7}	10^{-7}	0	0.1	100	10^{-5}	100	100	100	10^{-5}
X^-	−1	1.0	1.0	[c]	10^{-2}	0	[c]	100	0.001	100	100	100	0.001
R^-	−1	1.0	1.0	0	0	10^{-4}	0	0	0	0	0	0	0

[a] Calibration curves made for 0.01–10^{-12} mol/dm^3.
[b] Varies from 10^{-2} to 10^{-13} mol/dm^3.
[c] To provide electroneutrality.

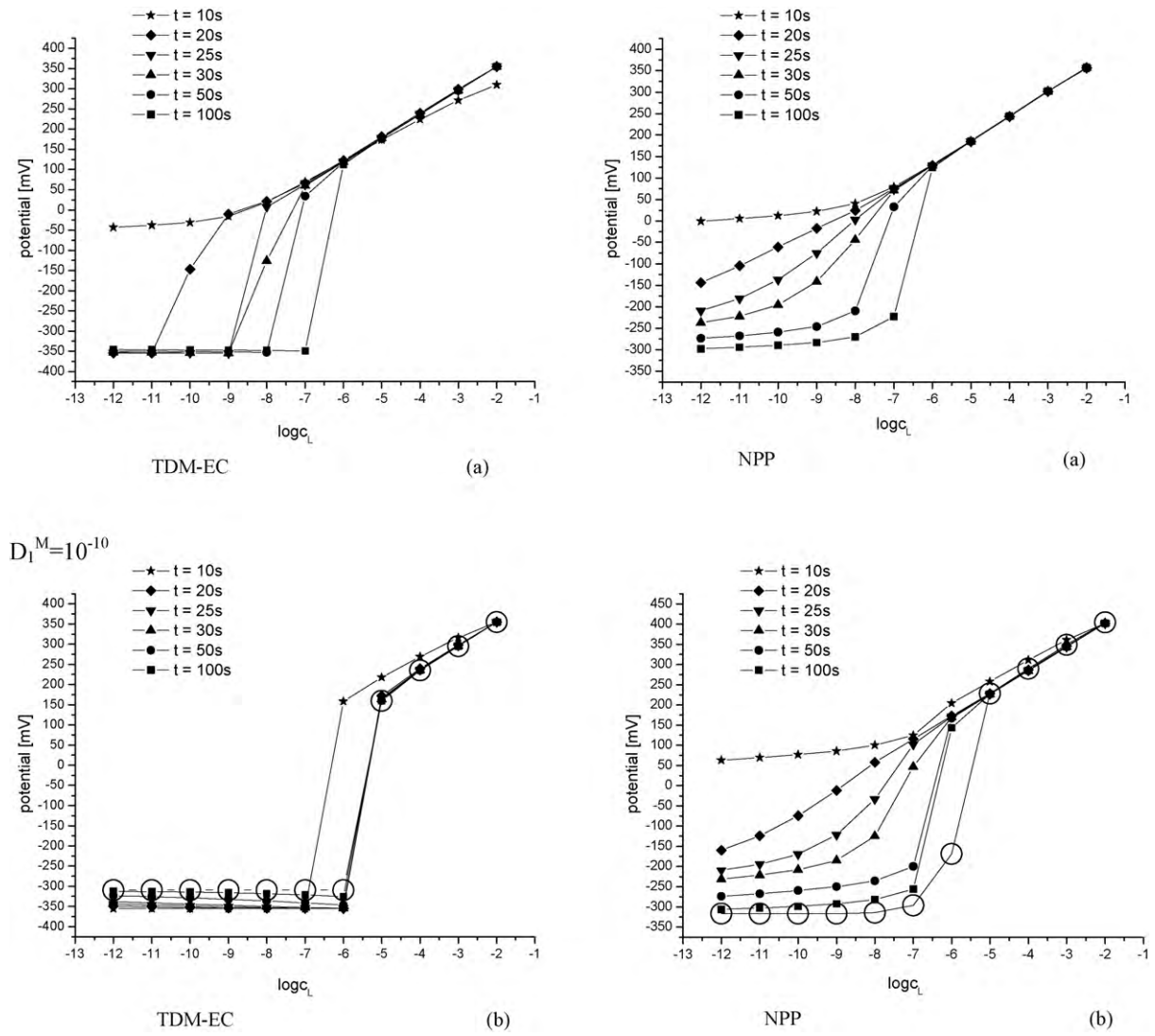

Fig. 1. Influence of measuring time for the ISE with preferred ion inner solution concentration 10^{-10} obtained using the TDM-EC (left) and the NPP (right) model. (a) Equal diffusion coefficients (above), (b) different diffusion coefficients $D_I = 10 \cdot D_J$ (below). Steady-state curves marked with empty circles.

"abrupt", the NPP curves are "smoother" and more similar to the experimental ones.

The cases described above are of the "normal problem" type (What is the value of the detection limit if we have a certain set of parameters?). Equally, or maybe more, important is the so-called "inverse problem" namely "Which set of parameters produces the best detection limit?"

The answer to this problem is illustrated in Fig. 2a which shows contour plot of the detection limit vs. the measurement time and the concentration of the primary ion in the inner solution (DL–*t*–[I]).

The concentration of I is plotted on the *x*-axis, the measuring time on the *y*-axis and the resulting value of the detection limit on the *z*-axis. The detection limit is depicted with the help of different colour intensities; the darker the colour, the lower the detection limit. The local/global minima can be read from the plot.

In order to obtain such contour plots, the measuring time was increased from 5 to 500 s with an interval of 5 s, and the ion concentration in the inner solution was varied over a range of 10 orders of magnitude (10^{-2} to 10^{-12} M) with an interval of one order of magnitude. For each calibration curve, eleven points were calculated. Thus, $100 \times 11 = 1100$ calibration curves and altogether 12 100 points had to be calculated. This is a "brute force" approach that requires a lot of computational effort, which is exponentially proportional to the number of investigated parameters. The process can be substantially speeded up by the use of more sophisticated techniques such as hierarchical genetic strategy (HGS) [32,33].

A look at the contour plots in Fig. 2a also reveals that while the models generally show the same tendency their results substantially differ in detail. In practice, TDM-EC displays only one global minimum (IS5, steady-state). In practice, TDM-EC displays only one global minimum. The model suggests that the best value of the detection limit (DL = $10^{-10.8}$) can be obtained with ISE5 using very long measuring times.

Simulations using NPP result in four local minima (of the value of DL) and one global. In simulations where the measuring time exceeds 5 min ($t > 300$ s) – and which are thus comparable to steady-state measurements – the lowest DL = $10^{-9.1}$ is obtained for ISE5.

In transient-state simulations, an even better DL = $10^{-10.6}$ can be noted for ISE6 ($t = 100$–200 s). A small, subnanomolar region DL = $10^{-9.9}$ occurs with ISE7 at $45\text{ s} < t < 50\text{ s}$, and another DL = 10^{-9} with ISE11 at $t = 25$ s. The latter could be very interesting in fast analysis, for example with automated clinical analyzers.

The results presented in Fig. 1a and b were obtained assuming that all species in water had the same diffusion coefficient and, sim-

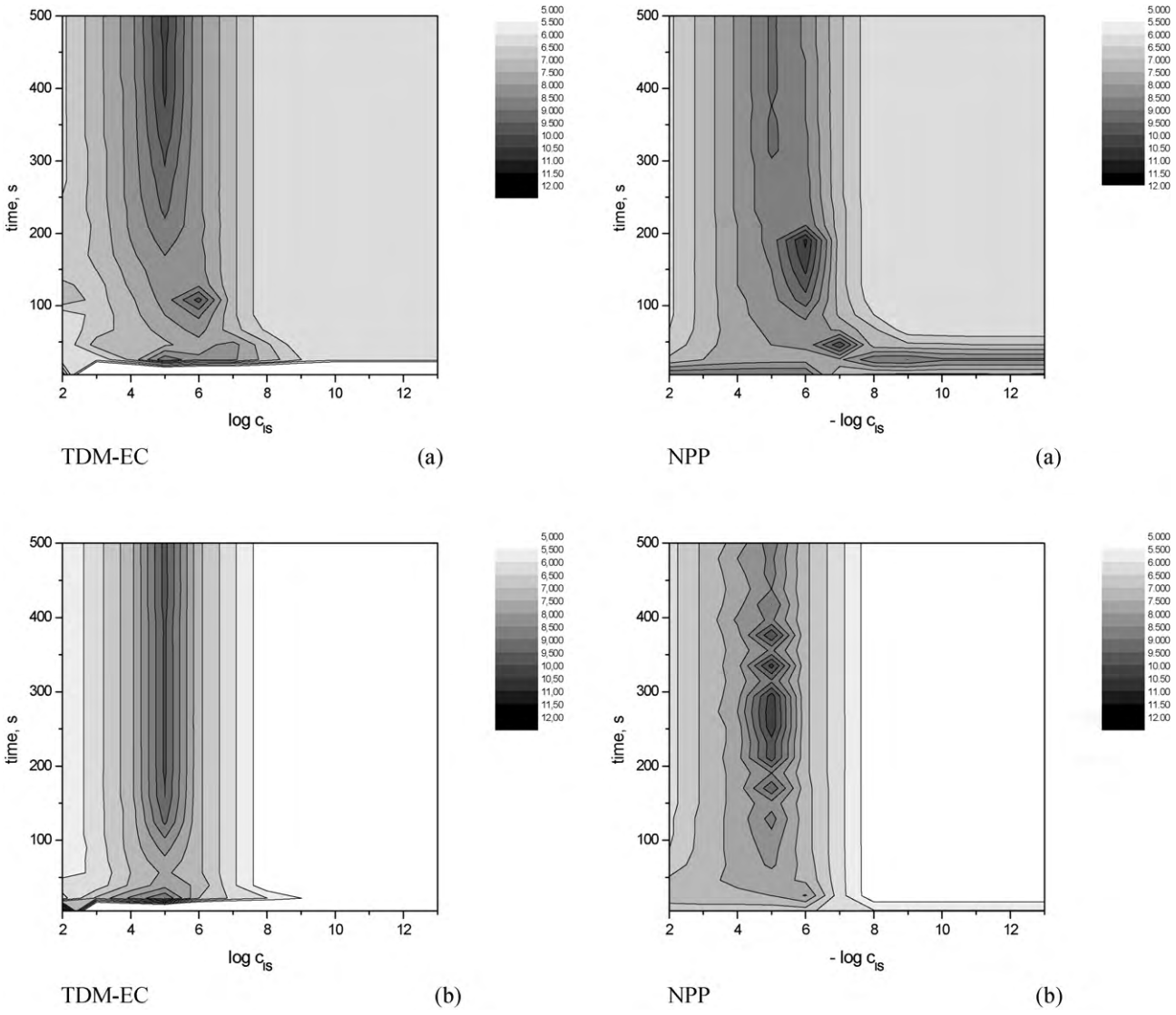

Fig. 2. The time–concentration-detection limit maps obtained using the TDM-EC (left) and the NPP (right) model. (a) Equal diffusion coefficients (above), (b) different diffusion coefficients $D_i = 10 \cdot D_j$ (below).

ilarly, that the diffusion coefficients of all species in the membrane were equal (see Table 2).

As we indicated above, the influence of different ionic diffusibility on the membrane potential formation was ignored by all models. The NPP model is a good tool to visualise this fact. Figs. 1b and 2b show the results obtained when assuming that the preferred ion has a 10 times higher diffusion coefficient in the membrane than the discriminated ion.

Now the difference in the predictions of TDM-EC and NPP is striking. TEM-EC predicts that the steady-state is reached almost immediately for $t > 10$ s. All curves, except those measured for 10 s, overlap each other and are the same as the steady-state curve (marked with empty circles). The NPP curves also show the influence of the faster transport of I, but this influence is considerably smaller. The curves for each measuring time length are still distinctly different from each other and different from the steady-state curve. This example nicely illustrates the effect of the potential formed inside the membrane (diffusion potential) on the evolution of the ISE signal. The electric field inside the membrane retards the transport of the faster moving ion and slows down the process of reaching steady-state.

This phenomenon is also seen very clearly in the contour plot (Fig. 2b). The map generated using the NPP model still resembles the one obtained for equal diffusion coefficients, although a faster transport effect is visible. The map obtained using the TDE-EC model shows that steady-state is reached very quickly for all I concentrations in the inner solution (vertical stripes on the plot).

4.2. Ions of different charges

In practical applications, ions of different charges are very often present in the solution. In such cases, the NPP is clearly superior to other models (see Table 1).

The experimental calibration curves of a calcium electrode, and the corresponding numerical simulations using the NPP model, are shown in Fig. 3. The experiment was made and described in Ref. [31]. The simulations were done using the parameters identical to that in [31]: two layers, $d_1 = 100$ μm, $d_2 = 200$ μm, $\varepsilon_1 = 7.07 \times 10^{-10}$, $\varepsilon_2 = 2.12 \times 10^{-10}$ (DOS + NPOE), $T = 298$ K (see Table 3). The time of each measurement was 1800 s. The NPP simulations were executed for a system containing six different ions. The inner solution concentrations for electrode A were: $c_{Ca^{2+}} = 10^{-2}$ M, $c_{H^+} =$

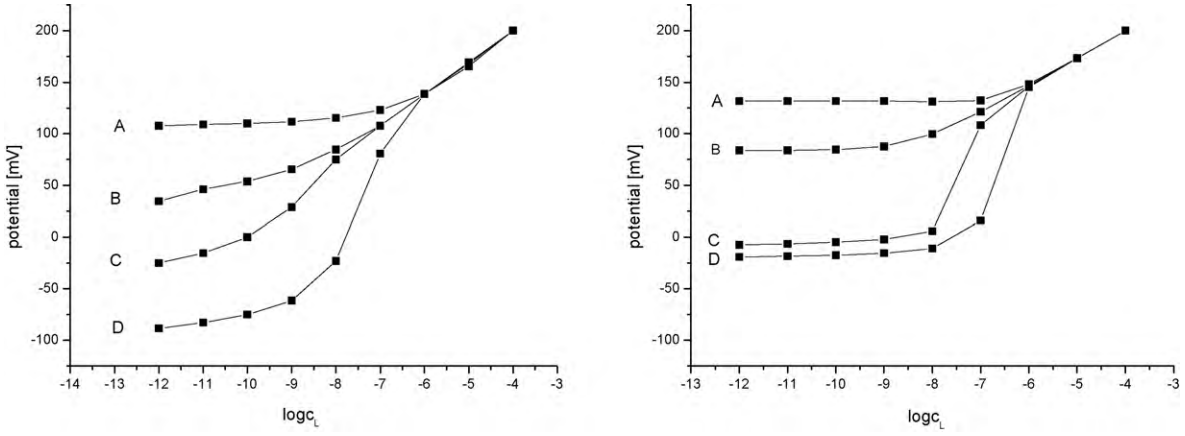

Fig. 3. Calcium electrode with a primary ion concentration in the inner solution equal to (A) 10^{-2} M, (B) 3×10^{-8} M, (C) 1.3×10^{-10} M, (D) 3×10^{-12} M. Experimental calibration curves (left) and theoretical curves obtained using the NPP model (right).

10^{-7} M, $c_{Na^+} = 0$; electrode B: $c_{Ca^{2+}} = 3 \times 10^{-8}$ M, $c_{H^+} = 4.07 \times 10^{-6}$ M, $c_{Na^+} = 0.073$ M; electrode C: $c_{Ca^{2+}} = 1.3 \times 10^{-10}$ M, $c_{H^+} = 1.2 \times 10^{-7}$ M, $c_{Na^+} = 0.1$ M; electrode D: $c_{Ca^{2+}} = 3 \times 10^{-12}$ M, $c_{H^+} = 2.5 \times 10^{-9}$ M, $c_{Na^+} = 0.12$ M. The number of discretization points was set to $N_1 = 60$ and $N_2 = 200$, and the first step of space discretization was set to 1×10^{-9}.

The resulting detection limits of the four electrodes used in the experiment were: (A) $c_{1,L} = 10^{-6.8}$ M, (B) $c_{1,L} = 10^{-8.5}$ M, (C) $c_{1,L} = 10^{-8.2}$ M, (D) $c_{1,L} = 10^{-6.3}$ M. The detection limits obtained in the NPP simulations were (A) $c_{1,L} = 10^{-6.9}$ M, (B) $c_{1,L} = 10^{-7.6}$ M, (C) $c_{1,L} = 10^{-7.3}$ M, (D) $c_{1,L} = 10^{-6.3}$ M. The differences may be caused by the fact that the experimental values of the layer thicknesses and the diffusion coefficients inside the membrane were unknown. The

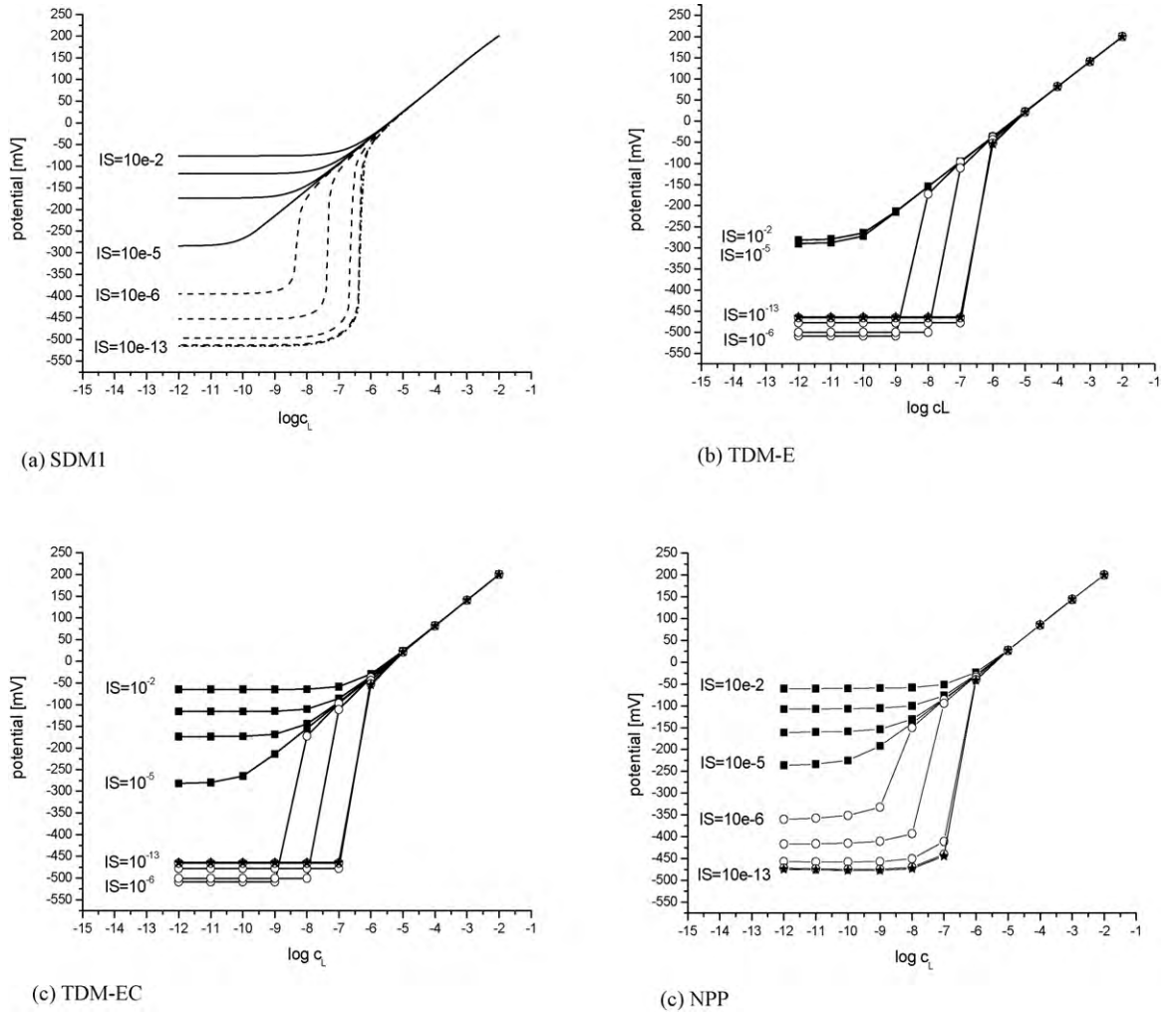

Fig. 4. The influence of the concentration of preferred ion in the inner solution. Calibration curves obtained using the (a) SDM1; (b) TDM-E; (c) TDM-EC; and (d) NPP models.

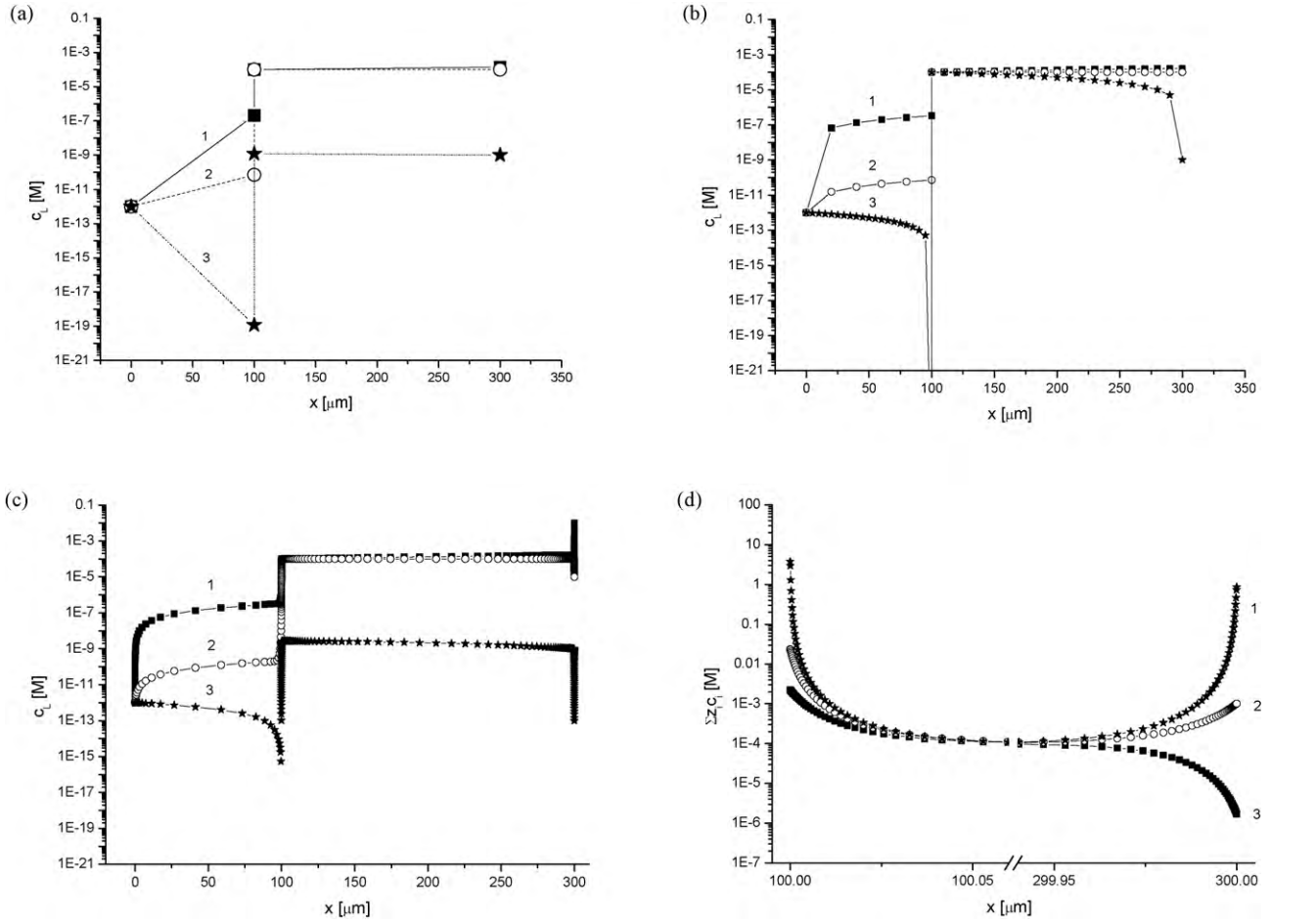

Fig. 5. Concentration profiles of (a–c) the preferred ion (I) (d) anionic sites (R^-) at the end of a virtual experiment. The concentration of I in the bulk of the solution is 10^{-13} M and in the inner filling solution (1) 10^{-2} M, (2) 10^{-5} M, (3) 10^{-13} M, respectively. The results were obtained using: (a) SDM1; (b) TDM-EC; (c) NPP and (d) NPP.

presence of additional ions in the solution, the leaching of the ionic sites, drift or other processes which were not considered in these particular simulations may also have had some effect. Nevertheless this case is a very good example of a successful application of the model to the complicated real-world example of ISE behaviour at low concentrations.

4.3. Steady-state comparison

The results obtained using SDM1 and SDM2 models give identical results so for the sake of brevity only the SDM1 results are discussed later.

Fig. 4a shows that by decreasing the concentration of the preferred ion (I) in the internal solution (IS), the detection limit can be improved by a few orders of magnitude towards the sub-nanomolar range. However, the decrease of [I] below a certain value (IS < 10^{-5} M) induces a strong, apparently super-Nernstian response because the sample ions in the diffusion boundary layer are depleted.

Similar results as for SDM1 were obtained using the TDM-EC model (Fig. 4c). Also, the TDM-E (Fig. 4b) model shows similar results for the curves which display super-Nernstian behaviour, but different ones for the curves which should have a higher than optimal detection limit. This is understandable, since the TDM-E model does not take coextraction processes into account, and therefore cannot model the worsening of the detection limit caused by the leakage of the preferred ion into the diffusion layer.

Fig. 5 shows space–concentration plots for different models. All three models show the same tendencies. The concentration of I at the membrane surface (a) is higher than in the bulk of the solution (for high [I] in the internal solution), (b) then decreases gradually with the decrease of I in the IS, and (c) eventually becomes lower than in the bulk of the solution (for low [I] in the IS). It should be

Table 3
Ion properties used for simulations of a calcium electrode (concentrations in mol/dm^3 and all other values in SI units).

i	z_i	D_i^1 [$\times 10^{-9}$]	D_i^2 [$\times 10^{-11}$]	c_{iL}	c_{iM}^1	c_{iM}^2	c_{iR}	$\vec{k}_{i\lambda_0}$	$\vec{k}_{i\lambda_1}$	$\vec{k}_{i\lambda_2}$	$\overleftarrow{k}_{i\lambda_0}$	$\overleftarrow{k}_{i\lambda_1}$	$\overleftarrow{k}_{i\lambda_2}$
Ca^{2+}	+2	0.798	0.798	[a]	10^{-4}	2.52×10^{-3}	[b]	1.0	10^{-4}	10^{-3}	1.0	10^{-3}	10^{-4}
Cl^-	−1	2.01	2.01	[c]	2×10^{-4}	0	[b]	1.0	5×10^{-8}	10^{-4}	1.0	10^{-4}	5×10^{-8}
H^+	+1	9.32	0.0932	10^{-7}	10^{-7}	0	[b]	1.0	2.8×10^{-6}	10^{-3}	1.0	10^{-3}	2.8×10^{-6}
Na^+	+1	1.35	1.35	0	0	0	[b]	1.0	6.85×10^{-8}	10^{-3}	1.0	10^{-3}	6.85×10^{-8}
$TFPB^-$	−1	0.1	0.1	0	0	5.04×10^{-3}	[c]	0	0	0	0	0	0

[a] Calibration curves made for 10^{-3} to 10^{-12} mol/dm^3.
[b] Different for each electrode.
[c] To provide electroneutrality.

noted that although SDM and TDM assume constant concentration of R inside the membrane, the NPP model shows that the concentration of R changes within the membrane, particularly close to the membrane boundaries.

These results show the agreement between the models as well as the agreement between the models and the experimental data.

Although SDM and TDM-EC are simplified models, which do not apply to complex practical cases (polyvalent ions, more than two ions, time influence), they compare satisfactorily with the general NPP model. The trends found using the SDM and the TDM-EC are confirmed by the NPP and are of general validity for the construction of low detection limit ISEs.

In the rest of this paragraph we will compare only NPP and SDM.

We studied the influence of the following parameters on the detection limit: the concentration of the discriminated ion [J], (a) in the sample and (b) in the internal solution, (c) the value of

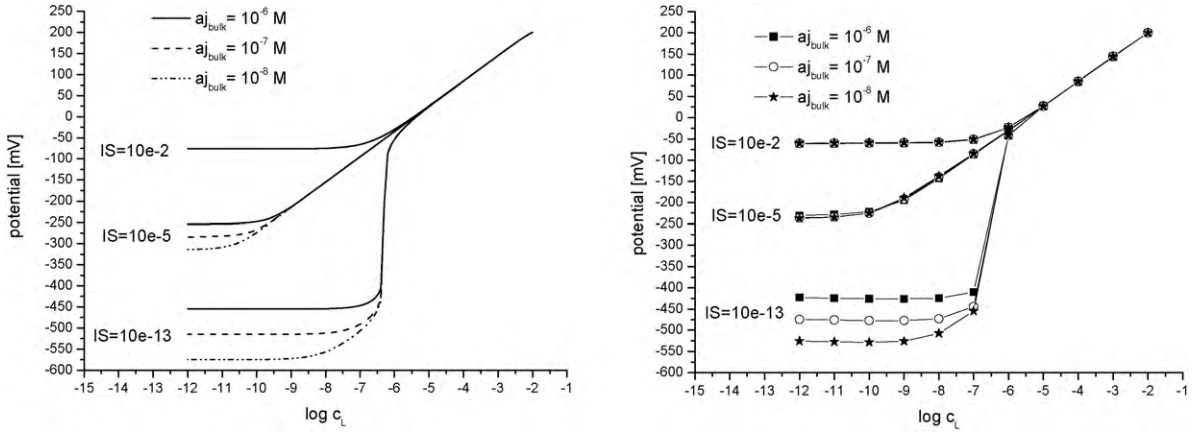

Fig. 6. The influence of the discriminated ion concentration in the sample. Calibration curves obtained using the SDM1 (left) and the NPP model (right).

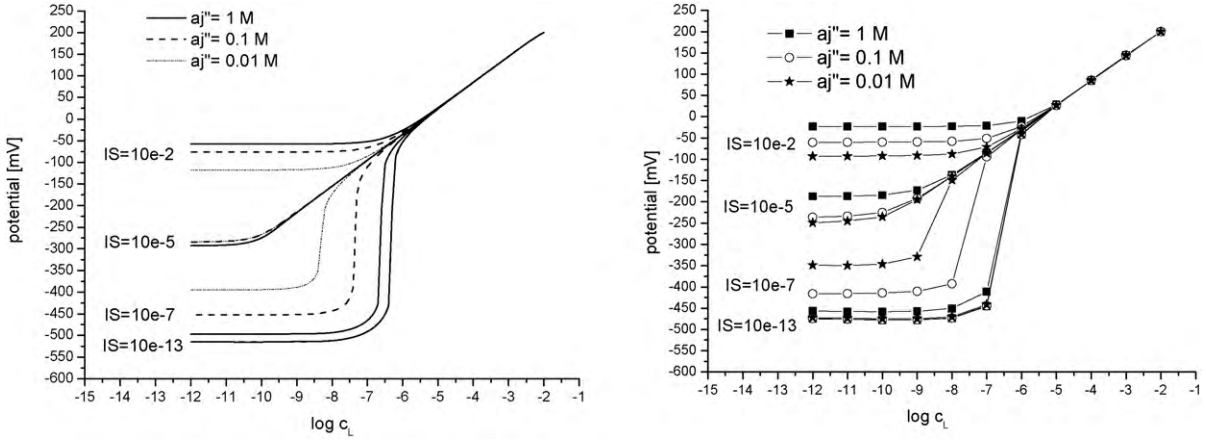

Fig. 7. Influence of the discriminated ion concentration in the internal solution. Calibration curves obtained using the SDM1 (left) and NPP (right) models.

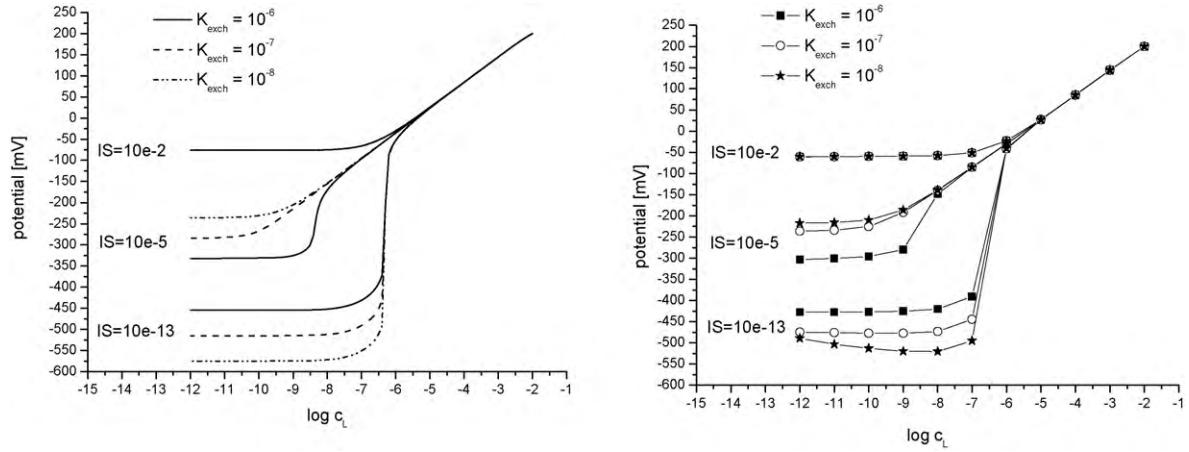

Fig. 8. Influence of the exchange constant. Calibration curves obtained using the SDM1 (left) and NPP models (right).

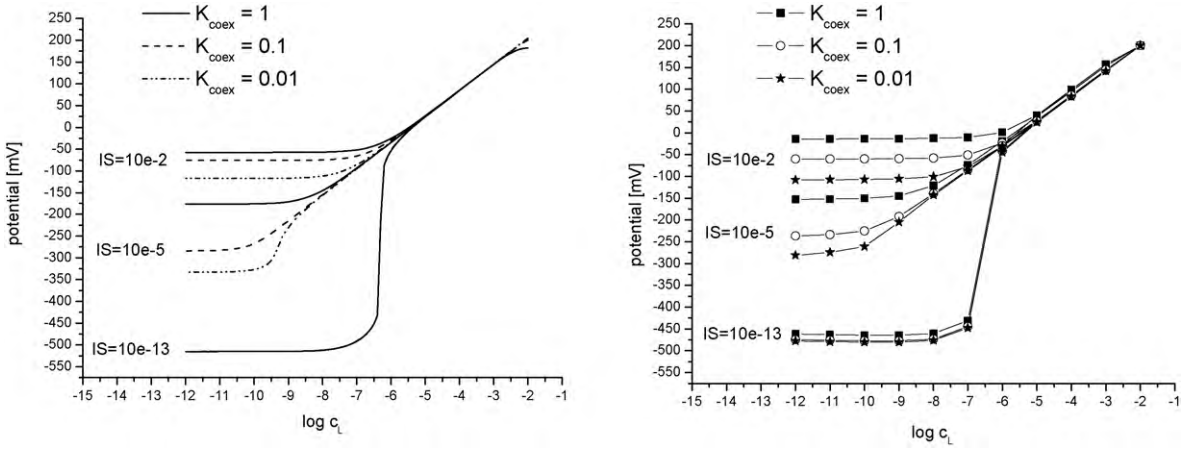

Fig. 9. Influence of the coextraction constant. Calibration curves obtained using the SDM1 (left) and NPP model (right).

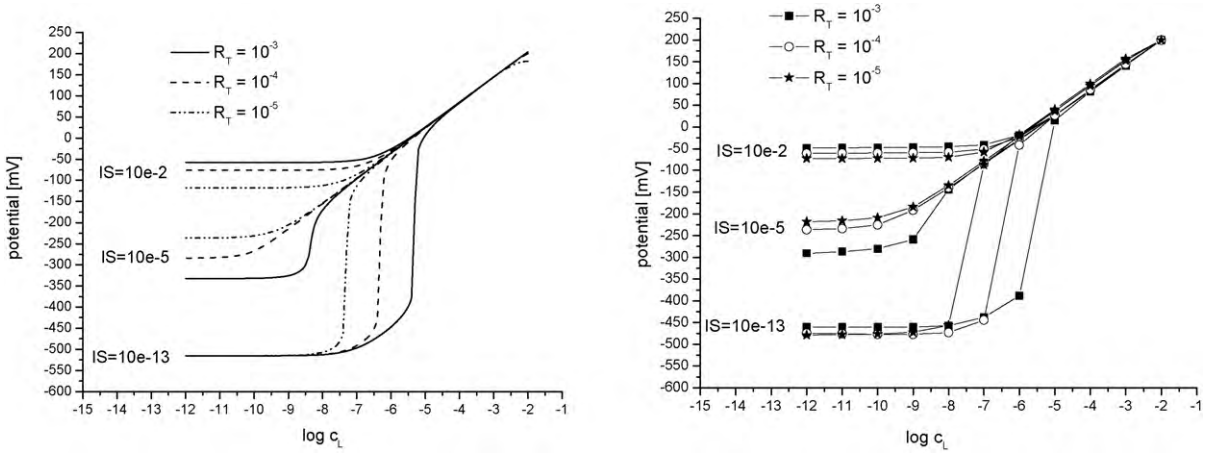

Fig. 10. Influence of ionic sites concentration. Calibration curves obtained using the SDM1 (left) and NPP model (right).

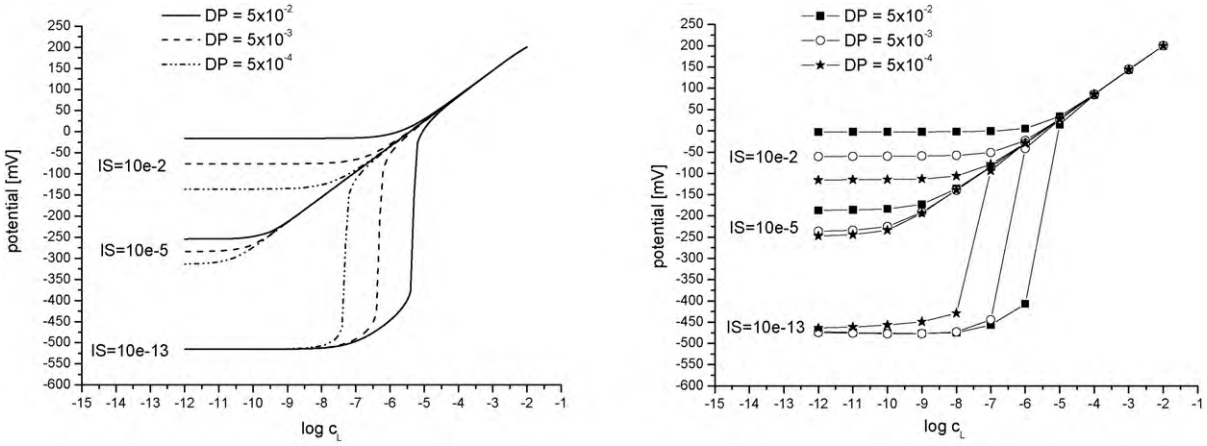

Fig. 11. Influence of diffusion coefficients. Calibration curves obtained using the SDM1 (left) and NPP model (right).

the exchange reaction constant, (d) the value of the coextraction reaction constant (e) the total concentrations of ion-exchanger sites and (f) transport parameters. Below, we focus on electrodes with the following concentrations of I in the inner solution: (a) 10^{-2} M, (denoted later as ISE2), which corresponds to a conventional system; (b) 10^{-5} M (ISE5), which generates the optimal steady-state response, and (c) 10^{-13} M (ISE13) with the strongest super-Nernstian response.

(a) The concentration of the discriminated ion in the sample, J, (Fig. 6) has the biggest effect on ISE13. The change in [J] by one order of magnitude induces a shift of the super-Nernstian plateau by 59 mV. The SDM simulations for ISE5 show, that the discriminated ion has an indirect influence on preventing the preferred ion from leaching to the sample. The NPP model predicts that this influence is negligible for ISE5. For ISE2, the influence of [J] in the sample is negligible, since the leaching of

I induces its high and constant concentration at the membrane surface.

(b) For ISE2 and ISE7, both models show that lowering [J] in the inner solution causes a small improvement of the detection limit (Fig. 7). For ISE5 NPP shows a similar effect, while SDM does not. For ISE13, both models predict that a lowering of [J] does not affect the detection limit.

(c) The exchange constant K_{exch} can be described as:

$$K_{\text{exch}} = \frac{\vec{k}_{J,\lambda_1}}{\vec{k}_{I,\lambda_1}} \cdot \frac{\overleftarrow{k}_{I,\lambda_1}}{\overleftarrow{k}_{J,\lambda_1}} = \frac{\overleftarrow{k}_{J,\lambda_2}}{\overleftarrow{k}_{I,\lambda_2}} \cdot \frac{\vec{k}_{I,\lambda_2}}{\vec{k}_{J,\lambda_2}} \tag{14}$$

For the NPP simulations, the values of $\vec{k}_{I,\lambda_1} = \vec{k}_{I,\lambda_2}$ were varied in the range of 10^{-6} to 10^{-4}. This, according to Eq. (14), results in values of K_{exch} in the 10^{-8} to 10^{-6} range (Fig. 8). With both models, a 10-fold increase of K_{exch} for ISE13 causes the potential of the super-Nernstian plateau to increase but has no effect on the detection limit. The effect is different on ISE5, for which the Nernstian response can change to super-Nernstian. The influence of K_{exch} on the detection limit of ISE2 is negligible.

(d) The coextraction constant K_{coex} can be described as:

$$K_{\text{coex}} = \frac{\vec{k}_{X^-,\lambda_1} \cdot \overleftarrow{k}_{I,\lambda_1}}{\overleftarrow{k}_{X^-,\lambda_1} \cdot \vec{k}_{I,\lambda_1} \cdot c^2_{R^-,M}} = \frac{\overleftarrow{k}_{X^-,\lambda_2} \cdot \vec{k}_{I,\lambda_2}}{\vec{k}_{X^-,\lambda_2} \cdot \overleftarrow{k}_{I,\lambda_2} \cdot c^2_{R^-,M}} \tag{15}$$

For the NPP simulations, the values of $\vec{k}_{X^-,\lambda_1} = \overleftarrow{k}_{X^-,\lambda_2}$ were varied in the 10^{-4} to 10^{-2} range which, according to Eq. (15), leads to values of K_{coex} within the 0.01–1 range. Both models predict a similar influence of K_{coex} on the detection limit (Fig. 9). The influence of K_{coex} on the detection limit of ISE13 is negligible. The decrease of K_{coex} improves the detection limit of ISEs with a Nernstian type of response (ISE2–ISE5). Decreasing K_{coex} below a certain value causes the Nernstian response of ISE5 to change into super-Nernstian, resulting in a worsening of the detection limit.

(e) The average anionic site concentration (R_T) in the membrane is equal to its initial concentration in the membrane ($c^2_{R^-,M}$), because an anionic site cannot enter or leave the membrane. This concentration was varied in the 10^{-3} to 10^{-5} M range (Fig. 10). When $c^2_{R^-,M}$ was increased/decreased in the NPP simulations, the heterogeneous rate constants $\vec{k}_{X^-,\lambda_1} = \overleftarrow{k}_{X^-,\lambda_2}$ were decreased/increased in order to keep K_{coex} constant (see Eq. (15)). A 10-fold decrease of R_T lowers the detection limit of ISE13 by one order of magnitude. For ISE5, a decrease of R_T causes the super-Nernstian response to change to Nernstian. According to the NPP model, the influence of R_T on ISE2 is negligible, while SDM predicts a small improvement of the detection limit with the decrease of R_T.

(f) The diffusion parameter (DP), which represents the influence of diffusion coefficients in water and in the membrane as well as the thickness of both layers, can be expressed as $\text{DP} = D^2_i d_1 / D^1_i d_2$. In the SDM and NPP model simulations, all diffusion coefficients in the membrane (D^2_i) were varied in the 10^{-10} to 10^{-12} m^2/s range. Both models predict that the increase of DP causes a lowering of the detection limit of all ISEs (Fig. 11).

5. Summary and conclusions

Three models describing the behaviour of ISEs (SDM, TDM-EC, and NPP) were compared both for transient and steady-state response.

Transient-state NPP simulations show the influence of time on the detection limits. For electrodes in which the outward flux of the preferred ion is either under-compensated or ideally compensated, the detection limit decreases with the increase of time. For electrodes in which the outward flux of the preferred ion is over-compensated, the detection limit decreases (improves) with the increase of time, reaches an optimum and then increases (worsens) again because of the super-Nernstian response (Fig. 1, NPP (a)). For transient-state measurements, much lower (subnanomolar) detection limits can be achieved than for steady-state measurements (Fig. 2).

The difference between the predictions of TDM-EC and NPP was demonstrated. It was especially pronounced in the case of unequal diffusion (Fig. 1, TDM-EC (b) and NPP (b)). TEM-EC predicts that the steady-state is reached almost immediately. The NPP predicts that the system will obtain steady-state more slowly. This example nicely illustrates the role of the potential formed inside the membrane (diffusion potential) on the ISE signal evolution. The electric field inside the membrane retards the transport of the faster moving ion thus slowing down the process of reaching steady-state. Here we have proof that the more general NPP model quantitatively reflects the important facts that arbitrary are not considered by simpler models.

Correspondingly, the use of NPP shows when simplifications are justified. In the case of steady-state and monovalent ions the tendencies shown by the SDM were confirmed with NPP simulations. The agreement between these two models is very good. Decreasing the concentration of the preferred ion in the inner solution, as well as the coextraction constant (anion lipophilicity), improves the detection limit by several orders of magnitude towards the subnanomolar range. After reaching an optimal value with a further decrease of one of these two parameters, the detection limit worsens and a super-Nernstian response is observed. When the parameters – e.g. the concentration of the discriminated ion in the inner solution, the ionic site concentration, or the diffusion (DP) parameter – are changed, different types of ISE behaviour is observed. The decrease of these parameter values leads to a lower detection limit for all electrodes. To design an electrode with the lowest possible detection limit, the parameter values should also be as low as possible. The exchange constant and the concentration of J in the bulk of the solution have little influence on electrodes with a nearly optimal concentration of preferred ion in the inner solution. Neither do they significantly affect the level of the super-Nernstian plateau for electrodes which show this type of response.

The NPP model is by far the most general of the models discussed (big number of components, polyvalent ions, transient-state potential measurements) and can be used for the description of a much wider range of phenomena concerning ISEs than the SDM or the TDM-EC models. It is also a tool to justify the use of simpler models in certain situations.

Acknowledgements

This work is a part of the MASTRA MATERA ERA-NET project funded under the 6th FP EU. Financial support from the Polish State Committee for Scientific Research (KBN) R15 005 03, as well as from Graduate School in Chemical Engineering is gratefully acknowledged.

Appendix A.

These equations have been converted into a set of dimensionless equations with the following transformations:

$$\bar{x} := \frac{x}{x_S}, \quad \bar{t} := \frac{t}{t_S}, \quad \bar{c}^j_i(\bar{x},\bar{t}) := \frac{c^j_i(x_S\bar{x}, t_S\bar{t})}{c_S}, \quad \bar{E}^j(\bar{x},\bar{t}) := \frac{E^j(x_S\bar{x}, t_S\bar{t})}{E_S}, \tag{A.1}$$

where x, t, c^j_i, E^j and $\bar{x}$, $\bar{t}$, $\bar{c}^j_i$, $\bar{E}^j$ are physical and dimensionless values of distance, time, concentration and electric field,

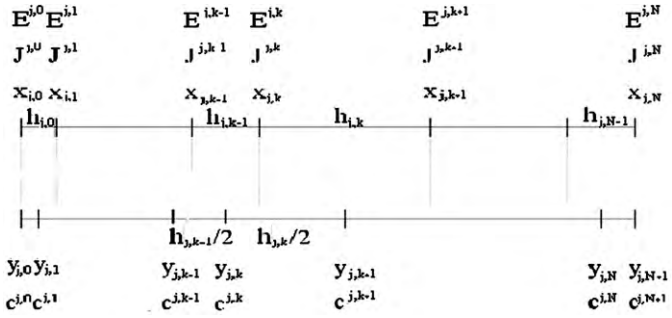

Fig. A.1. Space grid for the electro-diffusion problem for each phase α_j, where $J_i^{j,k}(t) = J_i(x_{j,k}, t)$, $c_i^{j,k}(t) = c_i(y_{j,k}, t)$.

respectively; x_S, t_S, c_S, E_S are their constant characteristic values. From this point on we use rescaled variables in equations. To ease the burden of notation the overbars are dropped.

Now the dimensionless model of electro-diffusion of r species can be described by the following set of equations:

$$\begin{cases} \dfrac{\partial c_i^j}{\partial t} = -\dfrac{\partial}{\partial x} J_i^j \quad \text{for } i = 1, \ldots, r, \\ \dfrac{\partial E^j}{\partial t} = I(t) - \lambda_j \displaystyle\sum_{i=1}^{r} z_i J_i^j, \end{cases} \tag{A.2}$$

where the rescaled flux is given as $J_i^j = -D_i^j(\partial c_i^j/\partial x) + \gamma z_i D_i^j c_i^j E^j$, D_i – rescaled diffusion coefficient, λ, γ are defined by: $\lambda_j = c_S x_S F/(E_S \varepsilon_j)$, $\gamma = F E_S x_S/(RT)$ and F, R, T, ε_j have their usual meaning (Faraday constant, gas constant, absolute temperature and dielectric permittivity in phase α_j). The influence of drift is neglected.

A.1. Numerical method

The method of lines [11], which requires space discretization only, was employed to numerically solve the problem above. We use a non-uniform grid denser near boundaries. Because of grid non-uniformity, the finite differences method with properly selected weights must be applied [12,34].

Fig. A.1 shows the space grid used in all phases α_j. The concentrations are defined at points $y_{j,k}$ while the fluxes and electric fields at points $x_{j,k}$. Each point $y_{j,k}$ is placed in the middle of the interval $[x_{j,k-1}, x_{j,k}]$.

The flux J_i^j gradient at point $y_{j,k}$ (for $k = 1, \ldots, N$) can be evaluated using the expression for the first derivative:

$$\left.\frac{\partial J_i^j}{\partial x}\right|_{y_{j,k}} = \frac{J_i^{j,k} - J_i^{j,k-1}}{h_{j,k-1}} \tag{A.3}$$

At the boundary nodes ($k = 0$, $k = N+1$), one-sided expressions for right- and left-side derivative are used:

$$\begin{aligned} \left.\frac{\partial J_i^j}{\partial x}\right|_{y_{j,0}} &\approx \frac{-h_{j,1}(2h_{j,0} + h_{j,1})J_i^{j,0} + (h_{j,0} + h_{j,1})^2 J_i^{j,1} - h_{j,0}^2 J_i^{j,2}}{h_{j,0}h_{j,1}(h_{j,0} + h_{j,1})}, \\ \left.\frac{\partial J_i^j}{\partial x}\right|_{y_{j,N+1}} &\approx \frac{h_{j,N-1}^2 J_i^{j,N-2} - (h_{j,N-1} + h_{j,N-2})^2 J_i^{j,N-1} + h_{j,N-2}(h_{j,N-2} + 2h_{j,N-1})J_i^{j,N}}{h_{j,N-1}h_{j,N-2}(h_{j,N-2} + h_{j,N-1})}. \end{aligned} \tag{A.4}$$

This leads to the formulation of a set of ordinary differential equations (ODE) defined by unknown functions $c_i^{j,k}(t)$, which have values in every point $y_{j,k}$, (where $k = 0, \ldots, N+1$) and $E^{j,k}(t)$, which have values in every point $x_{j,k}$ (where $k = 0, \ldots, N$):

$$\begin{aligned} \frac{dc_i^{j,0}}{dt} &= \frac{-h_{j,1}(2h_{j,0} + h_{j,1})J_i^{j,0} + (h_{j,0} + h_{j,1})^2 J_i^{j,1} - h_{j,0}^2 J_i^{j,2}}{h_{j,0}h_{j,1}(h_{j,0} + h_{j,1})}, \\ \frac{dc_i^{j,k}}{dt} &= -\frac{J_i^{j,k} - J_i^{j,k-1}}{h_{j,k-1}}, \\ \frac{dc_i^{j,N+1}}{dt} &= \frac{h_{j,N-1}^2 J_i^{j,N-2} - (h_{j,N-1} + h_{j,N-2})^2 J_i^{j,N-1} + h_{j,N-2}(h_{j,N-2} + 2h_{j,N-1})J_i^{j,N}}{h_{j,N-1}h_{j,N-2}(h_{j,N-2} + h_{j,N-1})}, \\ \frac{dE_i^{j,k}}{\partial t} &= I^j(t) - \Lambda^j \sum_{i=1}^{r} z_i J_i^{j,k} \end{aligned} \tag{A.5}$$

where $J_i^{j,k} = -D_i^j(\partial c_i^{j,k}/\partial x) + \gamma z_i D_i^j c_i^{j,k+\frac{1}{2}} E^j$. The space derivative of the concentration at y_k was approximated by a three-point, non-uniform finite difference:

$$\frac{dc_i^{j,k}}{dx} = 2\frac{h_{j,k-1}^2 c_i^{j,k+1} - h_{j,k}^2 c_i^{j,k} + (h_{j,k} - h_{j,k-1})(h_{j,k}c_i^{j,k} + h_{j,k-1}c_i^{j,k+1})}{h_{j,k-1}h_{j,k}(h_{j,k-1} + h_{j,k})} \tag{A.6}$$

and $c_i^{j,k+(1/2)}$ is the concentration at x_k with a weighted linear combination of the neighbouring concentrations as follows:

$$c_i^{j,k+(1/2)} \approx \frac{(h_{j,k}c_i^{j,k} + h_{j,k-1}c_i^{j,k+1})}{(h_{j,k-1} + h_{j,k})} \tag{A.7}$$

The boundary conditions take the form:

$$J_i^{j,N} = J_i^{j+1,0} = \vec{k}_{i\lambda_j} c_i^{j,N} - \overleftarrow{k}_{i\lambda_j} c_i^{j+1,0}(\lambda_j, t) \tag{A.8}$$

The above discretization leads to a system of ODEs in time variable. Due to the stiff nature of these ODEs, a special integrator is needed. We have used StiffIntegratorT, an implicit integrator based on the RADAU5 [35] procedure.

The electrical potential, which is an integral from electrical field over space can be expressed using the method of trapezes:

$$\begin{aligned} \varphi^{j,k} &= -\sum_{g=1}^{k} \left(\frac{1}{2}(E^{j,g} + E^{j,g-1})h_{j,g-1}\right), \\ \Delta\varphi &= \sum_{j=1}^{n} \varphi^{j,N} = -\sum_{j=1}^{n}\sum_{g=1}^{N} \left(\frac{1}{2}(E^{j,g} + E^{j,g-1})h_{j,g-1}\right). \end{aligned} \tag{A.9}$$

The NPP multilayer model (along with rescaling, discretization and data structures) as well as JEDS (a freeware computer program, which is a C++ implementation of the presented model and can be used in a number of applications), was described in details in Ref. [14].

Appendix B.

Let us denote the concentrations at the boundary as: c_i inside and c_i' outside the membrane. The set of equations for exchange, coextraction and electroneutrality

$$\begin{aligned} K_{\text{exch}} &= \frac{c_1' \cdot c_2}{c_1 \cdot c_2'} \\ K_{\text{coex}} &= \frac{c_1 \cdot c_3}{c_1' \cdot c_3'} \\ c_1 + c_2 &= c_3 + R_{\text{T}}, \quad c_1' + c_2' = c_3' \end{aligned} \tag{B.1}$$

can then be transformed into the form:

$$\begin{aligned} &\left(1 + K_{\text{exch}}\frac{c_2'}{c_1'}\right) c_1{}^2 + R_{\text{T}} \cdot c_1 + c_1'(c_1' + c_2')K_{\text{coex}} = 0 \\ &c_2 = c_1 \cdot K_{\text{exch}}\frac{c_2'}{c_1'} \end{aligned} \tag{B.2}$$

where Δ from the quadratic Eq. (B.2)

$$\Delta = R_T^2 + 4\left(1 + K_{exch}\frac{c_2'}{c_1'}\right)c_1'(c_1' + c_2')K_{coex} \tag{B.3}$$

is always higher than R_T^2, which means that it has one positive and one negative solution. The positive solution takes the form:

$$c_1 = \frac{R_T + \sqrt{\Delta_1}}{2 + 2K_{exch}(c_2'/c_1')} \tag{B.4}$$

Applying the Eqs. (B.2)–(B.4) to the left ($c_i = c_i^{2,0}$, $c_i' = c_i^{1,N}$) and right ($c_i = c_i^{2,N}$, $c_i' = c_{i,R}$) leads to Eqs. (12) and (13).

References

[1] J. Bobacka, A. Ivaska, A. Lewenstam, Chem. Rev. 108 (2008) 329.
[2] A. Radu, A.J. Meir, E. Bakker, Anal. Chem. 76 (2004) 6402.
[3] H. Cohen, J.W. Cooley, Biophys. J. 5 (1965) 145.
[4] J.R. Sandifer, R.P. Buck, J. Phys. Chem. 79 (1975) 384.
[5] T.R. Brumleve, R.P. Buck, J. Electroanal. Chem. 90 (1978) 1.
[6] T. Sokalski, A. Lewenstam, Electrochem. Commun. 3 (2001) 107.
[7] T. Sokalski, P. Lingenfelter, A. Lewenstam, J. Phys. Chem. B 107 (2003) 2443.
[8] P. Lingenfelter, I. Bedlechowicz-Sliwakowska, T. Sokalski, M. Maj-Zurawska, A. Lewenstam, Anal. Chem. 78 (2006) 6783.
[9] T. Sokalski, W. Kucza, M. Danielewski, A. Lewenstam, Anal. Chem. 81 (2009) 5016.
[10] P. Lingenfelter, T. Sokalski, A. Lewenstam, Unbiased selectivity coefficients: new insights from the Nernst–Planck–Poisson model, in: International Conference on Electrochemical Sensors MATRAFURED 2005, Mátrafüred, Hungary, 13-11-2005, 2005.
[11] W.E. Schiesser, The Numerical Method of Lines: Integration of Partial Differential Equations, Academic Press, San Diego, 1991.
[12] R. Filipek, Polish Ceram. Bull. 90 (2005) 103.
[13] W. Kucza, M. Danielewski, A. Lewenstam, Electrochem. Commun. 8 (2006) 416.
[14] J. Jasielec, Master Thesis, AGH-UST/ÅAU, 2008, http://web.abo.fi/jjasiele.
[15] B. Grysakowski, B. Bozek, M. Danielewski, Electro-diffusion in multi-component ion-selective membranes; numerical solution of the coupled Nernst–Planck–Poisson equations, Diffus. Defect Data, Pt. A 273–276[Diffusion in Solids and Liquids III] (2008) 113.
[16] H.C. Chang, G. Jaffe, J. Chem. Phys. 20 (1952) 1071.
[17] A. Hulanicki, A. Lewenstam, Talanta 24 (1977) 171.
[18] A. Lewenstam, Doctoral Thesis, Warsaw University, 1977.
[19] J. Crank, Mathematics of Diffusion, Oxford University Press, 1970.
[20] M.E. Glicksman, Diffusion in Solids: Field Theory, Solid-State Principles and Applications, John Wiley and Sons, 2000.
[21] J.S. Kirkaldy, D.J. Young, Diffusion in the Condensed State, The Institute of Metals, London, 1985.
[22] A. Lewenstam, A. Hulanicki, T. Sokalski, Anal. Chem. 59 (1987) 1539.
[23] M. Maj-Zurawska, T. Sokalski, A. Hulanicki, Talanta 35 (1988) 281.
[24] W.E. Morf, E. Pretsch, N.F. de Rooij, Theory and computer simulation of the time-dependent selectivity behavior of polymeric membrane ion-selective electrodes, J. Electroanal. Chem. 614 (1–2) (2008) 15.
[25] W.E. Morf, E. Pretsch, N.F. de Rooij, J. Electroanal. Chem. 602 (2007) 43.
[26] T. Sokalski, T. Zwickl, E. Bakker, E. Pretsch, Anal. Chem. 71 (1999) 1204.
[27] T. Zwickl, T. Sokalski, E. Pretsch, Electroanalysis 11 (1999) 673.
[28] W.E. Morf, M. Badertscher, T. Zwickl, N.F. de Rooij, E. Pretsch, J. Phys. Chem. B 103 (1999) 11346.
[29] T. Sokalski, A. Ceresa, T. Zwickl, E. Pretsch, J. Am. Chem. Soc. 119 (1997) 11347.
[30] T. Sokalski, E. Pretsch, Low detection limit ion selective membrane electrodes, Orion Research, Inc., USA, 98-US15217[9905515], 24-19990204. 1-1-1998. WO. 23-7-1998.
[31] T. Sokalski, A. Ceresa, M. Fibbioli, T. Zwickl, E. Bakker, E. Pretsch, Anal. Chem. 71 (1999) 1210.
[32] R. Schaefer, J. Kolodziej, R. Gwizdala, J. Wojtusiak, How simpletons can increase the community development - an attempt to hierarchical genetic computation, in: Proceedings of the 4th Conference on Evolutionary Algorithms and Global Optimization, 5–8 June 2000, Ladek Zdroj. 5-6-2000, 2000, p. 187.
[33] B. Wierzba, A. Semczuk, J. Kolodziej, R. Schaefer, Hierarchical genetic strategy with real number encoding, in: Proceedings of the 6th Conference on Evolutionary Algorithms and Global Optimization, 26–28 May 2003, Lagow, 2003.
[34] V.M. Volgin, A.D. Davydov, J. Electroanal. Chem. 600 (2007) 171.
[35] E. Hairer, G. Wanner, J. Comput. Appl. Math. 111 (1999) 93.